# Effects of Octahedral Tilting on Band Structure and Thermoelectric Power Factor of Titanate Perovskites: A First-Principles Study on $SrTiO_3$

Tianqi Zhao[†], Luke M. Daniels[‡], Ben Slater[†], Matthew J. Rosseinsky[‡], Furio Corà[*,†]

[†]Department of Chemistry, University College London, Gower Street, London, WC1E 6BT, United Kingdom

[‡]Department of Chemistry, University of Liverpool, 51 Oxford Street, Liverpool, L69 7ZD, United Kingdom

**ABSTRACT:** Doped $SrTiO_3$ and other perovskite structured titanates are attracting interest as n-type thermoelectric materials due to their relatively high thermoelectric power factor, low toxicity and modest cost. Taking $SrTiO_3$ as an exemplar, the effects of octahedral tilting on the electronic band structure and thermoelectric power factor of titanate perovskites have been studied from first-principles calculations. By utilizing Glazer's notation, six representative tilt systems, including three out-of-phase ($a^0a^0c^-$, $a^0b^-b^-$, and $a^-a^-a^-$) and three in-phase tilt systems ($a^0a^0c^+$, $a^0b^+b^+$, and $a^+a^+a^+$), were investigated. It is found that out-of-phase tilting improves the optimum power factor as compared to the cubic aristotype, while in-phase tilting marginally lowers the optimum power factor. The largest increase in power factor (~100%) is obtained in the one-tilt system $a^0a^0c^-$ at a tilt angle of 15°, which can be achieved with an energy cost of only 44 kJ $mol^{-1}$ per formula unit. These findings agree with the experimental evidence that increased power factors are found in $a^0a^0c^-$ and $a^-a^-a^-$ tilt systems of titanate perovskites. The predicted increase of Seebeck coefficient as a function of tilt angle in the $a^-a^-a^-$ tilt system of $SrTiO_3$ is also consistent with experimental increase of Seebeck coefficient in $a^-a^-a^-$ titanates of $La_{0.55}K_{0.45}TiO_3$ and $La_{0.5}Na_{0.5}Ti_{0.9}Nb_{0.1}O_3$. Our simulations provide valuable insights into tuning the thermoelectric power factor of titanate perovskite by controlling octahedral tilting.

## 1. INTRODUCTION

Thermoelectric materials enable the transformation of waste heat into usable electricity and are thus proposed as important contributors to the global energy management and environment protection.[1,2] Expanding the application of thermoelectric technology into the industrial setting, for example, sets strict requirements for both thermal and chemical stability that are not satisfied by the chalcogenide materials, such as $Bi_2Te_3$ alloys that are the current reference thermoelectrics.[3] In this context, oxide materials with higher chemical stability are attracting ever-increasing attention in thermoelectric applications.[4,5] The efficiency of a thermoelectric material can be quantified by the dimensionless figure of merit $ZT = S^2\sigma T/\kappa$, where $S$, $\sigma$, $\kappa$, and $T$ represent Seebeck coefficient, electrical conductivity, thermal conductivity, and absolute temperature, respectively. $S^2\sigma$ is further defined as thermoelectric power factor. Strontium titanate ($SrTiO_3$, STO) is a paradigmatic example of thermoelectric titanate perovskites, and provides a parent structure which upon n-type doping can produce a high power factor such as 28-36 $\mu$W $cm^{-1}$ $K^{-2}$ at room temperature in $Sr_{1-x}La_xTiO_3$ ($0.015 \le x \le 0.1$),[6] which is comparable to the commercial thermoelectric material $Bi_2Te_3$ alloys.[3] The $ZT$ of STO fails to reach unity, however, owing to the high thermal conductivity (~12 W $m^{-1}$ $K^{-1}$ at 300 K).[6,7] Significant focus has therefore been placed on reducing the thermal conductivity of STO through intrinsic approaches such as introducing cation and/or oxide vacancies,[8,9] nanostructuring approaches through reduced particle size,[10,11] engineering of the grain boundaries,[12] and incorporation of nanoinclusions.[13-15] The realization of phonon-glass electron-crystal (PGEC) behavior in titanate perovskite systems, such as $La_{0.5}Na_{0.5}Ti_{1-x}Nb_xO_3$, $La_{1-y}K_yTiO_3$ and $La_{0.5}K_{0.5}Ti_{1-x}Nb_xO_3$, achieves thermal conductivities as low as ~2.30 W $m^{-1}$ $K^{-1}$ at room temperature, which are 75%-80% lower than STO.[16,17] Following this incorporation of A site disorder, the power factor does not remain as high as STO; for example, the power factor of $La_{0.5}K_{0.5}Ti_{0.95}Nb_{0.05}O_3$ (~5 $\mu$W $cm^{-1}$ $K^{-2}$) is about one sixth that of La doped STO.[6,17] Therefore, despite substantial efforts and success in reducing the thermal conductivity, questions remain on how to best optimize the thermoelectric power factor of titanate perovskites.

With a stoichiometry of $ABO_3$, ideal perovskite oxides can be viewed as being formed of a cubic corner sharing $BO_6$ octahedral network, in which A sits the interstitial site in the center of eight $BO_6$ octahedra (Figure 1a). Variation in the size of either the A site or B site cations induce a range of structural distortions away from the highest symmetry cubic aristotype, rationalized through the Goldschmidt's tolerance factor, $t = (r_A + r_O)/[\sqrt{2}(r_B + r_O)]$.[18] Values of $t < 1$ result in octahedral tilting in the oxide lattice. STO adopts cubic $Pm\bar{3}m$ symmetry at room temperature. However, many other doped titanate perovskite phases adopt a tilt system at room temperature. $La_{0.55}K_{0.45}TiO_3$ and $La_{0.5}Na_{0.5}Ti_{0.9}Nb_{0.1}O_3$ are rhombohedral.[17] Rare-earth substituted STO undergo cubic to tetragonal change due to the decrease in ionic radii from $La^{3+}$ to $Y^{3+}$ in $Sr_{0.9}R_{0.1}TiO_{3\pm\delta}$, which exhibit high $ZT$ values of ~0.42 at 1200 K.[19] All but one material ($Sr_{0.9}La_{0.1}TiO_{3\pm\delta}$) adopt tetragonal symmetry ($I4/mcm$) as a result of $TiO_6$ octahedral tilting. Similar performance is achieved in the tetragonal system of $Sr_{1-3x/2}La_xTiO_{3-\delta}$ (with $x = 0.15$) which exhibits an optimum $ZT$ of 0.41

at 973 K and adopts $a^0a^0c^-$ symmetry.[20] In contrast, B site substituted titanate perovskite materials (e.g. incorporation of $Nb^{5+}$) typically retain the cubic $Pm\bar{3}m$ symmetry of undoped STO due to the larger ionic radius of the dopant cation, and exhibit *ZT* values of 0.2-0.4 at 1000 K.[21,22] Furthermore, it seen from these experiments that the increased power factor in these titanate perovskites might be correlated with octahedral tilting. For example, the power factors increase with tilt angle in $a^-a^-a^-$ tilt systems of $La_{0.55}K_{0.45}TiO_3$ (2.09 $\mu W$ $cm^{-1}$ $K^{-2}$ at 373 K, tilt angle 2.18°) and $La_{0.5}Na_{0.5}Ti_{0.9}Nb_{0.1}O_3$ (4.25 $\mu W$ $cm^{-1}$ $K^{-2}$ at 373 K, with tilt angle 7.45°).[16,17] The power factor is found to be dependent on cell volume and ionic radii of rare elements in the rare-earth substituted STO ($Sr_{0.9}R_{0.1}TiO_{3\pm\delta}$) with tetragonal cells,[19] which might also be related to the effects of octahedral titling.

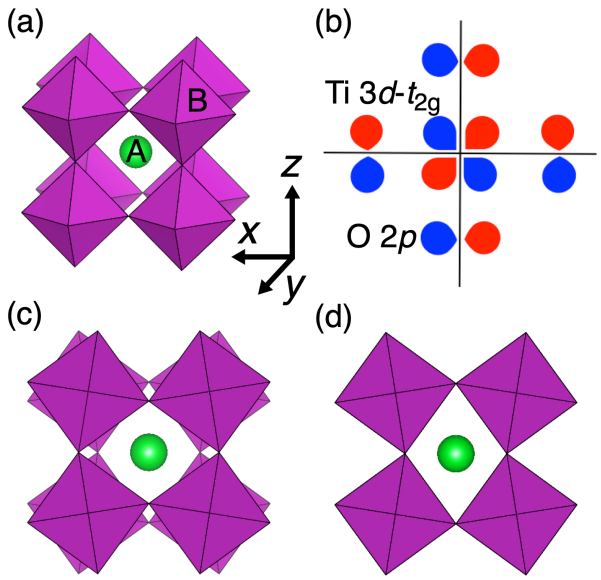


Figure 1. The crystal structure and octahedral tilting of perovskite oxide $ABO_3$. (a) Crystal structure of the cubic perovskite $ABO_3$. (b) Schematic model of the bonding between Ti 3*d*-$t_{2g}$ and O 2*p* frontier orbitals. (c) The top view of out-of-phase octahedral tilting around *z* axis. (d) The top view of in-phase octahedral tilting around *z* axis.

As shown in Figure 1b, the frontier orbitals of STO are formed of Ti 3*d*-$t_{2g}$ and O 2*p* orbitals. Therefore, electronic transport is mediated within the octahedral network by the interaction between these orbitals.[23,24] Octahedral tilting in perovskites significantly affects the overlap between these atomic orbitals and hence electron coupling between lattice points, and in principle, offers the freedom to tune the electron energy contribution at a level of materials design as a result of the flexibility of the perovskite structure. However, such band engineering *via* octahedral tilting to tune the thermoelectric power factor in titanate perovskites has not been clearly revealed. The difficulty partly resides in that the effect of octahedral tilting and doping are entangled in real materials and their separate contributions to enhancing the power factor are difficult to isolate. Computational studies allow us to achieve this separation by calculating how the power factor varies in phases with known tilting but with the same chemical composition, which is what we set out to achieve in the current study. With the notable exception of $Pb^{2+}$, the contribution of orbitals from A-site cations to the edges of valence and conduction bands in titanate perovskites is negligible,[23] hence the study of octahedral tilting in STO is representative of changes induced by doping.

The standard way to describe octahedral tilting in perovskites is through Glazer's notation, in which three letters (a, b, c) are used to describe the relative tilt angles around the *x*, *y*, and *z* axes, and three superscripts (+, -, 0) are used to indicate the relative rotation direction between adjacent octahedral layers.[25] The superscript "+" ("-") stands for in-phase (out-of-phase) octahedral tilting, meaning that adjacent octahedral layers rotate in the same (opposite) direction as illustrated in Figure 1c and 1d, while "0" means no rotation. For example, the tilt system $a^0b^-b^-$ has the same out-of-phase tilt angle around the *y* and *z* axes but no tilting around the *x* axis. Here, we investigate from first-principles calculations the variation of electronic conductivity and Seebeck coefficients as a function of tilt system and extent of tilt angle in the titanate perovskite lattice using STO as an exemplar. This approach considers the electronic transport properties that are intrinsic to the material though it is acknowledged that extrinsic effects such as grain boundary resistance that are controlled by ceramic processing, can significantly affect material performance. The effects of octahedral tilting on band structure and thermoelectric power factor of six representative tilt systems, including three out-of-phase ($a^0a^0c^-$, $a^0b^-b^-$, $a^-a^-a^-$) which typically describe *I*4/*mcm*, *Imma*, and *R*$\bar{3}$*c* space group symmetries, respectively, and three in-phase tilt systems ($a^0a^0c^+$, $a^0b^+b^+$, $a^+a^+a^+$), which describe *P*4/*mbm*, *I*4/*mmm* and *Im*$\bar{3}$ symmetries, have been calculated by combining density functional theory (DFT) calculations and the semi-empirical Boltzmann transport formalism.

## 2. METHODS

DFT calculations were performed by utilizing CRYSTAL17 with the B1WC hybrid functional, which includes 16% Hartree-Fock exchange combined with the Wu-Cohen GGA exchange functional and Perdew-Wang correlation functional.[26,27] The B1WC hybrid functional was chosen because it has been verified to deliver a good description of both the lattice constants and band gap of STO.[28,29] The electron basis sets were chosen from the CRYSTAL online database (Sr_HAYWSC311(1d)G_piskunov_2004 for Sr, Ti_86411(1d)G_baranek_2013_BaTiO3 for Ti, and O_8411(1d)G_baranek_2013_BaTiO3 for O).[30] An 8 × 8 × 8 Monkhorst-Pack ***k*** grid was used in the optimization of the unit cell of STO with energy and force convergence criteria being $10^{-7}$ Hartree and $4.5 \times 10^{-4}$ Hartree/Bohr, respectively. The obtained cell parameter ($a$ = 3.884 Å) and band gap ($E_g$ = 3.59 eV) show good agreement with experimental results ($a$ = 3.905 Å, $E_g$ = 3.25 eV)[31,32] and previous computational results ($a$ = 3.880 Å, $E_g$ = 3.57 eV).[28] The obtained Ti-O bond length is 1.942 Å (= $a/2$). The band structure and density of states (DOS) of STO calculated with unit cell is shown in Figure S1. The obtained band width of the flat band in the Γ-X direction is 0.17 eV, compared to 0.25 eV in literature.[33]

We adopted Woodward's method[34] to build the aristotype ($a^0a^0a^0$) and six hettotype ($a^0a^0c^-$, $a^0b^-b^-$, $a^-a^-a^-$, $a^0a^0c^+$, $a^0b^+b^+$, $a^+a^+a^+$) STO structures based on the optimized unit cell, which is untilted. Structures corresponding to rotation of rigid $TiO_6$ octahedra have been generated using the code POTATO[35] that produces as output a 2 × 2 × 2 supercell expansion in $P\bar{1}$ symmetry of the tilted systems, which we have used without further modifications. The tilt angles were kept identical in different directions for simplicity and five tilt angles (3°, 6°, 9°, 12°, and 15°) were calculated. The structure and cell parameters for different tilt systems with tilt angle of 9° are shown and compared with the $a^0a^0a^0$ system (Table S1, Figure S2-S8). The $a^-a^-a^-$ system adopts a rhombohedral cell, there is an angle which derivates from 90° in $a^0b^-b^-$, and all other calculated tilt systems adopt orthorhombic cells. Self-consistent field calculations were performed for each tilt system with fixed cell parameters and atomic positions. The energy convergence was achieved to $10^{-7}$ Hartree on an 8 × 8 × 8 Monkhorst-Pack ***k*** grid. As the aristotype and hettotype systems are all based on the 2 × 2 × 2 supercell of STO, the original band structure of unit cell folds in the smaller first Brillouin zones. For example, the original flat band in the Γ-X direction of the unit cell becomes two flat bands along the Γ-X direction of the aristotype $a^0a^0a^0$ system (Figure 2a, Figure S1).

The Boltzmann transport equations as implemented in the code BoltzTraP2 were utilized to calculate the electrical conductivity $\sigma$ and Seebeck coefficient $S$:[36,37]

$$\sigma = \frac{e^2}{V}\int \tau_k v_k v_k \left(-\frac{\partial f_0(\varepsilon_k)}{\partial \varepsilon_k}\right) d\varepsilon \qquad (1)$$

$$S = \frac{e^2}{\sigma T}\int \tau_k v_k v_k \left(\varepsilon_k - \varepsilon_f\right)\left(-\frac{\partial f_0(\varepsilon_k)}{\partial \varepsilon_k}\right) d\varepsilon \qquad (2)$$

where $\varepsilon_k$, $v_k$, $\tau_k$, $\varepsilon_f$, $f_0$, $e$, $V$, $T$ are the electron energy, group velocity, relaxation time, Fermi energy, Fermi-Dirac distribution function, elementary charge, unit cell volume, and absolute temperature, respectively. The carrier concentration was calculated as:

$$n = N - \int g(\varepsilon) f_0(\varepsilon) d\varepsilon \qquad (3)$$

where $N$ is the total number of electrons in the unit cell, $g$ is the density of states. A fine ***k*** grid of 31 × 31 × 31 was used to obtain the electron energy based on the converged charge density. The electron energy was further interpolated on a denser ***k*** grid (× 10) in BoltzTraP2 to get converged values of thermoelectric coefficients. The influence of octahedral tilting on the relaxation time of the hypothetical tilted STO systems was omitted and a constant relaxation time was adopted for all tilt systems (4.3 fs by following a previous calculation of Bilc *et al.*).[28]

## 3. RESULTS AND DISCUSSION

The electronic band structure and DOS of the aristotype $a^0a^0a^0$ system of STO is shown in Figure 2a. The lowest conduction bands exhibit the distinctive flat-and-dispersive band features in the Γ-X direction. The coexistence of flat and dispersive bands can be demonstrated analytically using the tight-binding theory.[23,38]

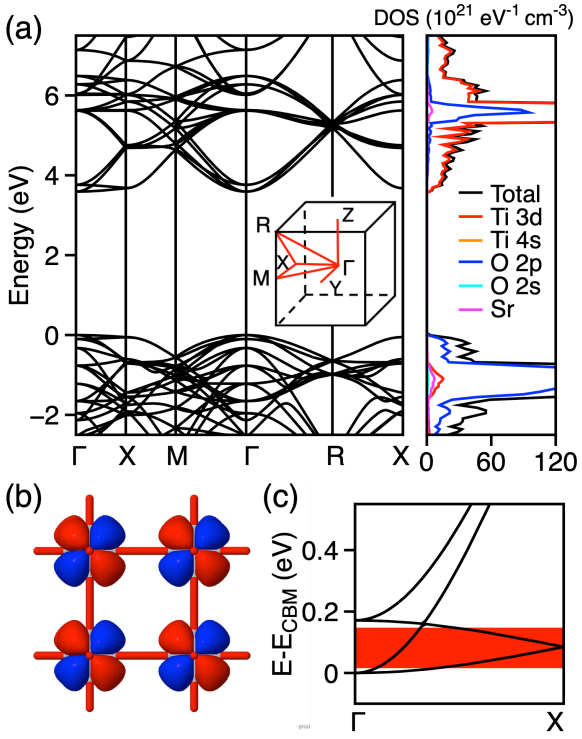


Figure 2. Electronic properties of aristotype $a^0a^0a^0$ system of STO. (a) Electronic band structure and DOS of the aristotype $a^0a^0a^0$ system of STO. Inset: the first Brillouin zone with high symmetry lines and points. (b) Crystal orbital of the conduction band minimum (CBM) at Γ. (c) Enlarged diagram showing the bottom of the conduction bands along Γ-X, with the energy of CBM set to zero. The red shaded area shows the Fermi energy range when the electron concentration is between 1 × $10^{20}$ cm$^{-3}$ and 1 × $10^{21}$ cm$^{-3}$ at 300 K in the rigid band approximation.

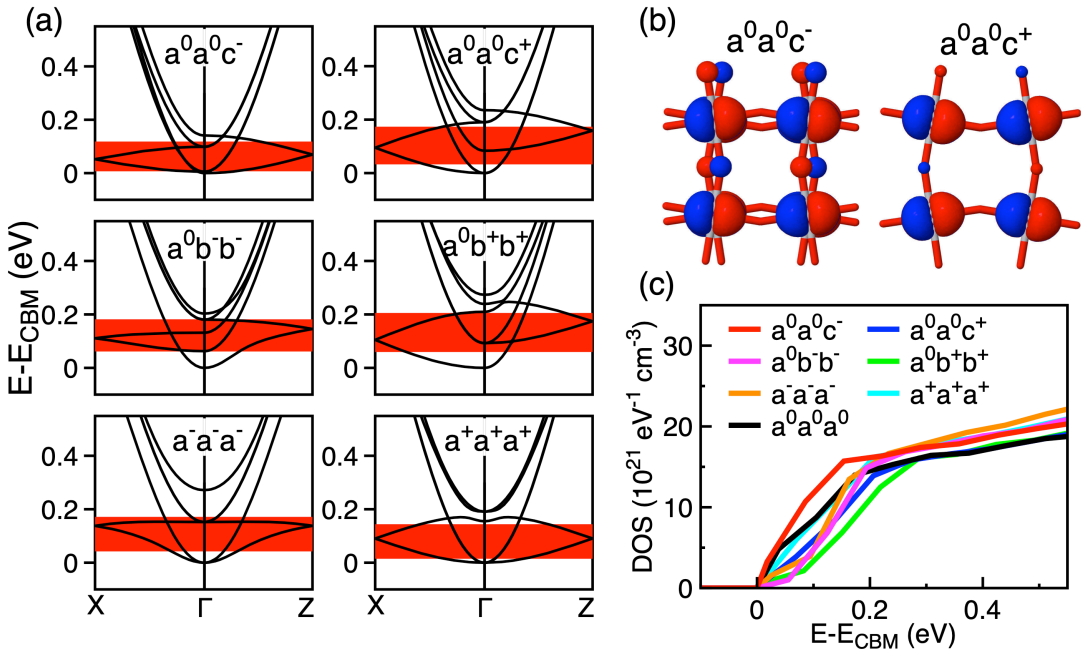


Figure 3. Electronic structure of six hettotype tilt system of STO: $a^0a^0c^-$, $a^0b^-b^-$, $a^-a^-a^-$, $a^0a^0c^+$, $a^0b^+b^+$, and $a^+a^+a^+$, with tilt angle of 9°. (a) The conduction bands of the six examined tilt systems of STO. The red shaded area is the Fermi energy range when the electron concentration is between $1 \times 10^{20}$ cm$^{-3}$ and $1 \times 10^{21}$ cm$^{-3}$ at 300 K in the rigid band approximation. (b) Crystal orbitals at Γ of the lowest conduction bands in $a^0a^0c^-$ and $a^0a^0c^+$ tilt systems of STO. (c) Density of states of six hettotype tilt systems of STO ($a^0a^0c^-$ in red, $a^0b^-b^-$ in purple, $a^-a^-a^-$ in yellow, $a^0a^0c^+$ in blue, $a^0b^+b^+$ in green, and $a^+a^+a^+$ in cyan) as compared to the aristotype $a^0a^0a^0$ system of STO (in black).

The high symmetry lines Γ-X, Γ-Y, and Γ-Z in the reciprocal space coincides with *x*, *y* and *z* directions in real space for cubic STO, respectively. Taking Ti 3$d_{yz}$ orbital as an example, it is orthogonal to the 2*p* orbitals of the two nearest neighbor oxygen atoms along *x*, and thus forms a non-bonding flat band in Γ-X direction; instead it couples with oxygen 2*p* orbitals in the *y* and *z* directions, generating dispersive bands in Γ-Y and Γ-Z direction (Figure 1b).Each of the three Ti 3*d*-$t_{2g}$ atomic orbitals yields a flat band in one reciprocal space direction and two dispersive bands in the other two directions. Conversely, in each reciprocal space direction there are one flat and two dispersive bands. For symmetry reasons, the oxygen 2*p* orbitals show no contribution to the lowest conduction bands due to the presence of bonding and anti-bonding couplings between Ti 3*d* and O 2*p* that cancel each other out. The electron state of CBM at Γ is three-fold degenerate without accounting for electron spin, which correspond to levels formed by non-bonding Ti 3*d*-$t_{2g}$ ($d_{xy}$, $d_{yz}$, $d_{xz}$) orbitals (Figure 2b).

As STO has been investigated extensively, we firstly performed benchmark calculations of the electrical transport properties of the cubic $a^0a^0a^0$ system. The effective masses $m^*$ of the flat and dispersive conduction bands were obtained by fitting parabola near the CBM through the formula:

$$E = E_{CBM} + \frac{\hbar^2 k^2}{2m^*} \qquad (4)$$

where $E$, $E_{CBM}$, and $\hbar$ are the electron energy, electron energy at CBM, and the reduced Planck constant, respectively. The effective masses of the flat and dispersive bands are calculated to be 6.1 $m_e$ and 0.42 $m_e$ ($m_e$ is the electron mass), respectively, which agree well with previous calculation (6.1 $m_e$ and 0.4 $m_e$).[28] The effective mass for heavy electrons is also in agreement with values obtained from measurements of the Seebeck coefficients (~6 $m_e$).[6,7] As has been pointed out by Shirai *et al.*,[33] the heavy and light electrons are responsible for high Seebeck coefficient and electrical conductivity in STO, respectively. Thus, the coexistence of flat and dispersive bands provides the best compromise between Seebeck coefficient and electrical conductivity. The Seebeck coefficient, electrical conductivity, and power factor of aristotype $a^0a^0a^0$ STO were calculated by using Boltzmann transport theory in the constant relaxation time and rigid band approximation (Figure S9). The electrical conductivity and absolute value of Seebeck coefficient have opposite trends as a function of carrier concentration, so an optimum power factor ($PF_{opt}$) is obtained at a specific carrier concentration. The n-type $PF_{opt}$ is calculated to be 9.8 $\mu$W cm$^{-1}$ K$^{-2}$ at 300 K for aristotype $a^0a^0a^0$ system when the carrier concentration is $4.3 \times 10^{20}$ cm$^{-3}$ (Figure S9). The obtained $PF_{opt}$ is lower than experimental values of 28-36 $\mu$W cm$^{-1}$ K$^{-2}$ measured in $Sr_{1-x}La_xTiO_{3-\delta}$ ($x$ = 0.015-0.1) single crystals at the same level of carrier concentration ($2.3 \times 10^{20}$ cm$^{-3}$ – $19.3 \times 10^{20}$ cm$^{-3}$).[6] The discrepancy between experimental and theoretical values might be due to the polaronic nature of electronic carriers in STO and cannot be described well by the rigid band approximation applied here. However, our results are consistent with previous calculations (~10 $\mu$W cm$^{-1}$ K$^{-2}$ at 300 K, ~14 $\mu$W cm$^{-1}$ K$^{-2}$ at 400 K).[28,39]

In the Boltzmann transport equation, the carrier concentration depends on Fermi energy and temperature through the Fermi-Dirac distribution. The carrier concentration can be obtained by applying Eq. (3) in the rigid band

approximation. Since doped STO materials are n-type semiconductors, we modified the Fermi energy around the conduction band edge to simulate electron doping. Figure 2c shows that the Fermi energy is within ~0.2 eV above the CBM when the carrier concentration is between $1.0 \times 10^{20}$ $cm^{-3}$ and $1.0 \times 10^{21}$ $cm^{-3}$ at 300 K. Thus, this concentration of carriers is accommodated within the total band width of the two flat bands at the bottom of the conduction bands at room temperature. Experimentally, strategies such as $La^{3+}$ doping on $Sr^{2+}$ site is utilized to increase carrier concentration in STO. For example, La doping in $Sr_{1-x}La_xTiO_3$ ($0.015 \leq x \leq 0.1$) induces carrier concentration of $(0.2\text{-}2) \times 10^{21}$ $cm^{-3}$.[6] It can therefore be concluded that electrical transport coefficients are mainly determined by band edge states within the total band width of the two flat bands at room temperature. For this reason, we shall highlight the bottom of conduction bands only following the rotational distortions of the perovskite phases.

Figure 3a shows the lowest conduction bands for the six hettotype STO systems in the energy range up to 0.55 eV above the CBM (set as zero of the energy). Since the Γ-Y direction is equivalent to Γ-X or Γ-Z in all considered tilt systems, the conduction bands are shown along Γ-X and Γ-Z directions only for simplicity. Octahedral tilting induces anisotropic band dispersion and band splitting near CBM in both of the out-of-phase and in-phase tilt systems. It is interesting to note that the total band width of the two flat bands decreases in all three out-of-phase tilt systems but increases in all three in-phase tilt system. In order to analyze this difference, the crystal orbitals at Γ of the lowest conduction bands in the $a^0a^0c^-$ and $a^0a^0c^+$ systems are shown in Figure 3b. It is indicated that the out-of-phase tilting induces larger anti-bonding between Ti 3*d* $t_{2g}$ and O 2*p* orbitals than in-phase tilting, which results in higher orbital localization and narrower band width. Figure 3a further shows that the Fermi energy is also within ~0.2 eV above CBM when the carrier concentration is between $1.0 \times 10^{20}$ $cm^{-3}$ and $1.0 \times 10^{21}$ $cm^{-3}$ at 300 K in the six hettotype tilt systems. The DOS of the aristotype $a^0a^0a^0$ and six hettotype STO systems in the energy range up to 0.55 eV above CBM are compared in Figure 3c. At ~0.2 eV above CBM, which is the Fermi energy for a carrier concentration of $\sim 1.0 \times 10^{21}$ $cm^{-3}$ at 300 K, the slope of DOS shows a significant dependence on the type of tilting. It is intriguing to observe that the slopes of DOS increase in all three out-of-phase tilt systems, but remain almost identical to $a^0a^0a^0$ in all three in-phase tilt systems. This is consistent with the smaller band width of the flat band at ~0.2 eV above CBM in the three in-phase tilt systems. According to the Mahan-Sofo theory, an increase in the slope of DOS around Fermi energy improves the Seebeck coefficient.[40] Thus, it is believed that out-of-phase tilt systems possess higher Seebeck coefficients than in-phase tilt systems and aristotype system.

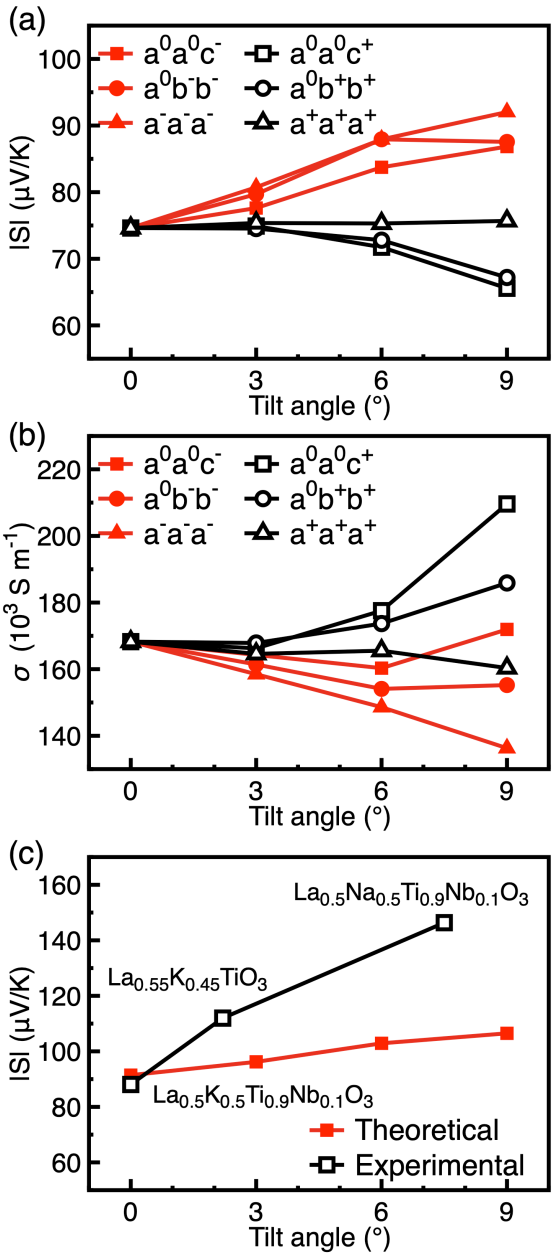


Figure 4. Variation of thermoelectric charge transport coefficients with octahedral tilting. Dependence of the absolute value of Seebeck coefficient (a) and electrical conductivity (b) as a function of tilt angle for six hettotype tilt systems in *z* direction when electron concentration is $1 \times 10^{21}$ $cm^{-3}$ at 300 K. (c) Comparison between theoretical and experimental dependence of the absolute value of Seebeck coefficient as a function of tilt angle for the $a^-a^-a^-$ tilt systems at 373 K.

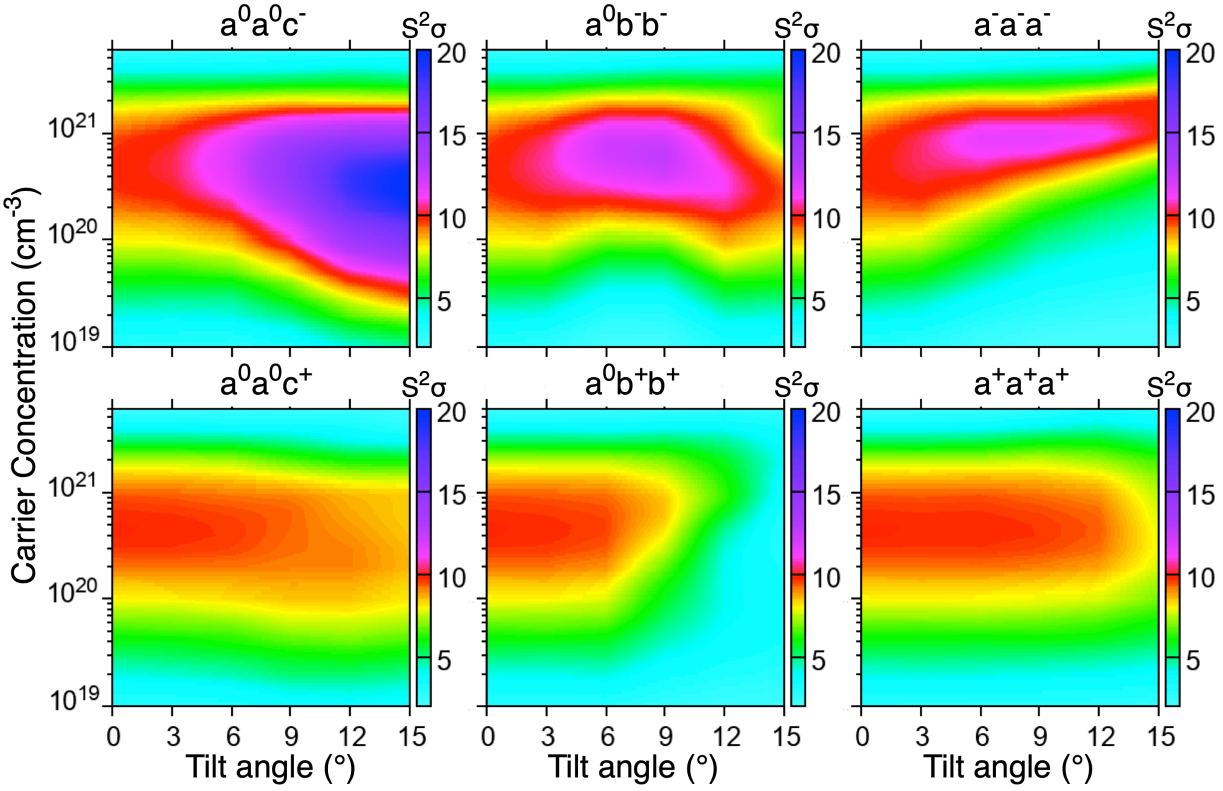


Figure 5. Dependence of power factor as a function of tilt angle and carrier concentration at 300 K in six hettotype tilt systems, i.e., three out-of-phase tilt systems: $a^0a^0c^-$, $a^0b^-b^-$, and $a^-a^-a^-$, and three in-phase tilt systems: $a^0a^0c^+$, $a^0b^+b^+$, and $a^+a^+a^+$ along *z* direction. The unit of power factor is $\mu$W cm$^{-1}$ K$^{-2}$.

The variation of the absolute value of Seebeck coefficient and electrical conductivity in *z* direction (chosen because *z* is the common direction around which octahedral tilting exists for all calculated one-, two-, and three-tilt systems) as a function of tilt angle are shown in Figure 4a and 4b, respectively, when carrier concentration is 1.0 × 10$^{21}$ cm$^{-3}$ at 300 K. It indicates that the absolute value of Seebeck coefficient increases as a function of tilt angle in all three out-of-phase tilt systems, in agreement with the trends predicted by the Mahan-Sofo theory.[40] However, the Seebeck coefficient decreases with increasing tilt angle in the three in-phase tilt systems. The electrical conductivity has an opposite dependence on tilt angle as compared to Seebeck coefficient for all tilt systems. The Seebeck coefficient and electrical conductivities have been measured experimentally for three different titanate perovskite single crystals with $a^-a^-a^-$ tilting, i.e., $La_{0.5}K_{0.5}Ti_{0.9}Nb_{0.1}O_3$ with no tilt angle, $La_{0.55}K_{0.45}TiO_3$ with 2.81° tilt angle, and $La_{0.5}Na_{0.5}Ti_{0.9}Nb_{0.1}O_3$ with 7.45° tilt angle, which are reproduced in Table S2.[16,17] As shown in Figure 4c, the dependence of Seebeck coefficient on tilt angle is in qualitative agreement with experiment results of the $a^-a^-a^-$ tilt systems. Although the effects of chemical configuration and the variation of carrier concentration cannot be excluded, our results indicate that out-of-phase tilting is beneficial for improving the absolute Seebeck coefficients in titanate perovskites. Unlike the electrical conductivity, the Seebeck coefficient is unaffected by extrinsic effects such as grain boundary resistance, which further increases the relevance of this approach to designing future thermoelectric materials.

Figure 5 shows the dependence of power factor as a function of tilt angle and carrier concentration in the six hettotype STO tilt systems at 300 K. The $PF_{opt}$ and the corresponding tilt angle, electrical conductivity, Seebeck coefficient, and carrier concentration at 300 K for the six hettotype systems are summarized in Table S2. The optimum carrier concentration for $PF_{opt}$ is (3.0-9.0) × 10$^{20}$ cm$^{-3}$ for all six hettotype tilt systems. As the increase of Seebeck coefficient is squared in thermoelectric power factor formulae ($PF = S^2\sigma$), the increase of Seebeck coefficient surpasses the decrease of electrical conductivity with increasing tilt angle in all three out-of-phase tilt systems, which results in higher power factor. The largest increase in power factor is achieved in the one-tilt system $a^0a^0c^-$ (~100% at tilt angle of 15°, i.e. 20.2 $\mu$W cm$^{-1}$ K$^{-2}$ vs. 9.8 $\mu$W cm$^{-1}$ K$^{-2}$). This result agrees with the evidence that increased power factor is found in doped STO materials with $a^0a^0c^-$ tilting.[19] However, further increase in tilt angle will cause the decrease of power factor in $a^0a^0c^-$ tilt system (Figure S10), which is caused by the decrease of Seebeck coefficients due to the significant band splitting between flat and dispersive bands when tilt angle is larger than 15° (Figure S11). The power factor has the largest increase of ~28% and ~17% in $a^0b^-b^-$ and $a^-a^-a^-$ tilt systems, respectively, when tilt angle is 9°. It is also noted that increased power factors can be achieved in the $a^0a^0c^-$ tilt system over wider range of carrier concentrations. The energy cost of the distortion as a function of tilt angle for the six hettotype tilt systems is shown in Figure S12. Rotation of the octahedra up to 9° incurs a penalty smaller than 100 kJ mol$^{-1}$ per formula unit for all tilt systems.

The energy variation for the one-tilt system $a^0a^0c^-$ that yields the best power factor is the lowest among all distortion examined, and amounts to 4 kJ mol$^{-1}$ at a tilt angle of 9° and 44 kJ mol$^{-1}$ at 15°. Such energy contributions are easily achievable through the defect chemistry associated with doping, and indeed experimental evidence shows that doping does modify the octahedral tilt. Experimentally, the increase of power factor with tilt angle at the same nominal carrier concentration is observed in the two rhombohedral $a^-a^-a^-$ materials, $La_{0.5}Na_{0.5}Ti_{0.9}Nb_{0.1}O_3$ and $La_{0.55}K_{0.45}TiO_3$ with tilt angle of 7.45° and 2.18°, respectively (Table S3).[17] Figure 5 also shows that the power factor decreases slowly as a function of tilt angle in all three in-phase tilt systems. The power factor decreases significantly when the tilt angle is larger than 9° and 15° in $a^0b^+b^+$ and $a^+a^+a^+$ tilt systems, respectively, which can be attributed to the much larger band splitting and band width (Figure S13).

## 4. CONCLUSIONS

These results enable us to clarify the possibility of optimizing thermoelectric power factor of titanate perovskites by controlling octahedral tilting. The effects of octahedral tilting on the electronic band structure and thermoelectric power factor in titanate perovskites have been studied from first-principles calculations using $SrTiO_3$ as an exemplar. It is found that out-of-phase tilting is beneficial for improving the Seebeck coefficient and power factor, while in-phase tilting lowers the thermoelectric power factor slowly with increasing tilt angle. The increase of power factor in out-of-phase tilt systems ($a^0a^0c^-$, $a^0b^-b^-$, $a^-a^-a^-$) is attributed to the increase of the slope of density of states around the Fermi energy. The most significant increase (~100%) of power factor occurs in $a^0a^0c^-$ one-tilt system when the tilt angle is 15° with energy cost of only 44 kJ mol$^{-1}$ per formula unit. These results agree with the experimental observation that increased power factor is found in $a^0a^0c^-$ and $a^-a^-a^-$ tilt systems of titanate perovskites.[16,17,19] The improved Seebeck coefficient of $a^-a^-a^-$ tilt systems as a function tilt angle is confirmed by experimental results collected from materials that adopt the same tilt system.[16,17] As such, both the octahedral tilt system and tilt angle are important factors that should be considered in optimizing the thermoelectric performance of titanate perovskite materials, with the one-tilt out-of-phase $a^0a^0c^-$ system identified as the superior symmetry and tilt system to achieve high thermoelectric power factor. In the context of titanate perovskite thermoelectrics, mechanisms of doping through the B site frequently retain the cubic ($a^0a^0a^0$) symmetry, whilst substitution through the A site often induced octahedral tilting.[19-22] Our study from first principles indicates that the tilt systems of $a^0a^0c^-$ and $a^-a^-a^-$, which often result from A site substitution,[16,20] provide the most promising routes to enhancing the thermoelectric power factor in titanate perovskites.

## ASSOCIATED CONTENT

### Supporting Information

The Supporting Information is available free of charge on the ACS Publications website.

Additional figures and tables, computational details, and references (PDF)

## AUTHOR INFORMATION


### Corresponding Author

*E-mail: f.cora@ucl.ac.uk (F. C.).


### Author Contributions

The manuscript was written through contributions of all authors. All authors have given approval to the final version of the manuscript.

### Notes

The authors declare no competing financial interest.

## ACKNOWLEDGMENT


We thank EPSRC for funding under EP/N004884. This work used the ARCHER UK National Supercomputing Service (http://www.archer.ac.uk)


## REFERENCES


(1) He, J.; Tritt, T. M., Advances in thermoelectric materials research: Looking back and moving forward. *Science* **2017,** *357*, eaak9997.

(2) Snyder, G. J.; Toberer, E. S., Complex thermoelectric materials. *Nat. Mater.* **2008,** *7*, 105-114.

(3) Witting, I. T.; Chasapis, T. C.; Ricci, F.; Peters, M.; Heinz, N. A.; Hautier, G.; Snyder, G. J., The thermoelectric properties of bismuth telluride. *Adv. Electron. Mater.* **2019,** *5*, 1800904.

(4) Hébert, S.; Berthebaud, D.; Daou, R.; Bréard, Y.; Pelloquin, D.; Guilmeau, E.; Gascoin, F.; Lebedev, O.; Maignan, A., Searching for new thermoelectric materials: Some examples among oxides, sulfides and selenides. *J. Phys.: Condens. Matter.* **2016,** *28*, 013001.

(5) He, J.; Liu, Y.; Funahashi, R., Oxide thermoelectrics: The challenges, progress, and outlook. *J. Mater. Res.* **2011,** *26*, 1762-1772.

(6) Okuda, T.; Nakanishi, K.; Miyasaka, S.; Tokura, Y., Large thermoelectric response of metallic perovskites: $Sr_{1-x}La_xTiO_3$ ($0 \leqslant x \leqslant 0.1$). *Phys. Rev. B: Condens. Matter Mater. Phys.* **2001,** *63*, 113104.

(7) Ohta, S.; Nomura, T.; Ohta, H.; Koumoto, K., High-temperature carrier transport and thermoelectric properties of heavily La- or Nb-doped $SrTiO_3$ single crystals. *J. Appl. Phys.* **2005,** *97*, 034106.

(8) Popuri, S. R.; Scott, A. J. M.; Downie, R. A.; Hall, M. A.; Suard, E.; Decourt, R.; Pollet, M.; Bos, J. W. G., Glass-like thermal conductivity in $SrTiO_3$ thermoelectrics induced by A-site vacancies. *RSC Adv.* **2014,** *4*, 33720-33723.

(9) Srivastava, D.; Norman, C.; Azough, F.; Schäfer, M. C.; Guilmeau, E.; Kepaptsoglou, D.; Ramasse, Q. M.; Nicotra, G.; Freer, R., Tuning the thermoelectric properties of A-site deficient $SrTiO_3$ ceramics by vacancies and carrier concentration. *Phys. Chem. Chem. Phys.* **2016,** *18*, 26475-26486.

(10) Wang, Y.; Fujinami, K.; Zhang, R.; Wan, C.; Wang, N.; Ba, Y.; Koumoto, K., Interfacial thermal resistance and thermal conductivity in nanograined $SrTiO_3$. *Appl. Phys. Express* **2010,** *3*, 031101.

(11) Park, K.; Son, J. S.; Woo, S. I.; Shin, K.; Oh, M.-W.; Park, S.-D.; Hyeon, T., Colloidal synthesis and thermoelectric properties of La-doped $SrTiO_3$ nanoparticles. *J. Mater. Chem. A* **2014,** *2*, 4217-4224.

(12) Ekren, D.; Azough, F.; Gholinia, A.; Day, S. J.; Hernandez-Maldonado, D.; Kepaptsoglou, D. M.; Ramasse, Q. M.; Freer, R., Enhancing the thermoelectric power factor of $Sr_{0.9}Nd_{0.1}TiO_3$ through control of the nanostructure and microstructure. *J. Mater. Chem. A* **2018,** *6*, 24928-24939.

(13) Wang, J.; Zhang, B.-Y.; Kang, H.-J.; Li, Y.; Yaer, X.; Li, J.-F.; Tan, Q.; Zhang, S.; Fan, G.-H.; Liu, C.-Y.; Miao, L.; Nan, D.; Wang, T.-M.; Zhao, L.-D., Record high thermoelectric performance in bulk $SrTiO_3$ via nano-scale modulation doping. *Nano Energy* **2017,** *35*, 387-395.

(14) Wang, N.; Chen, H.; He, H.; Norimatsu, W.; Kusunoki, M.; Koumoto, K., Enhanced thermoelectric performance of Nb-doped $SrTiO_3$ by nano-inclusion with low thermal conductivity. *Sci. Rep.* **2013,** *3*, 3449.

(15) Srivastava, D.; Norman, C.; Azough, F.; Schäfer, M. C.; Guilmeau, E.; Freer, R., Improving the thermoelectric properties of $SrTiO_3$-based ceramics with metallic inclusions. *J. Alloys Compd.* **2018,** *731*, 723-730.

(16) Daniels, L. M.; Savvin, S. N.; Pitcher, M. J.; Dyer, M. S.; Claridge, J. B.; Ling, S.; Slater, B.; Corà, F.; Alaria, J.; Rosseinsky, M. J., Phonon-glass electron-crystal behaviour by A site disorder in n-type thermoelectric oxides. *Energy Environ. Sci.* **2017,** *10*, 1917-1922.

(17) Daniels, L. M.; Ling, S.; Savvin, S. N.; Pitcher, M. J.; Dyer, M. S.; Claridge, J. B.; Slater, B.; Corà, F.; Alaria, J.; Rosseinsky, M. J., A and B site doping of a phonon-glass perovskite oxide thermoelectric. *J. Mater. Chem. A* **2018,** *6*, 15640-15652.

(18) Goldschmidt, V. M., Die gesetze der krystallochemie. Die *Naturwissenschaften* **1926,** *14*, 477-485.

(19) Kovalevsky, A. V.; Yaremchenko, A. A.; Populoh, S.; Thiel, P.; Fagg, D. P.; Weidenkaff, A.; Frade, J. R., Towards a high thermoelectric performance in rare-earth substituted $SrTiO_3$: Effects provided by strongly-reducing sintering conditions. *Phys. Chem. Chem. Phys.* **2014,** *16*, 26946-54.

(20) Lu, Z.; Zhang, H.; Lei, W.; Sinclair, D. C.; Reaney, I. M., High-figure-of-merit thermoelectric La-doped A-site-deficient $SrTiO_3$ Ceramics. *Chem. Mater.* **2016,** *28*, 925-935.

(21) Zhang, B.; Wang, J.; Zou, T.; Zhang, S.; Yaer, X.; Ding, N.; Liu, C.; Miao, L.; Li, Y.; Wu, Y., High thermoelectric performance of Nb-doped $SrTiO_3$ bulk materials with different doping levels. *J. Mater. Chem. C* **2015,** *3*, 11406-11411.

(22) Thong, T. Q.; Huong, L. T. T.; Tinh, N. T., Investigation of the influence of singly and dually doping effect on scattering mechanisms and thermoelectric properties of perovskite-type STO. *Mater. Trans.* **2015,** *56*, 1365-1369.

(23) Corà, F.; Alfredsson, M.; Mallia, G.; Middlemiss, D. S.; Mackrodt, W. C.; Dovesi, R.; Orlando, R. In *Structure and Bonding*; Mingos, D. M. P., Ed.; Springer, Berlin, 2004; The performance of hybrid density functionals in solid state chemistry, pp 171-232.

(24) Dylla, M. T.; Kang, S. D.; Snyder, G. J., Effect of two-dimensional crystal orbitals on Fermi surfaces and electron transport in three-dimensional perovskite oxides. *Angew. Chem. Int. Ed.* **2019,** *58*, 2-12.

(25) Glazer, A. M., The classification of tilted octahedra in perovskites. *Acta Cryst.* **1972,** *B28*, 3384-3392.

(26) Dovesi, R.; Erba, A.; Orlando, R.; Zicovich-Wilson, C. M.; Civalleri, B.; Maschio, L.; Rérat, M.; Casassa, S.; Baima, J.; Salustro, S.; Kirtman, B., Quantum-mechanical condensed matter simulations with CRYSTAL. *Wiley Interdiscip. Rev.: Comput. Mol. Sci.* **2018,** *8*, e1360.

(27) Bilc, D. I.; Orlando, R.; Shaltaf, R.; Rignanese, G. M.; Íñiguez, J.; Ghosez, P., Hybrid exchange-correlation functional for accurate prediction of the electronic and structural properties of ferroelectric oxides. *Phys. Rev. B: Condens. Matter Mater. Phys.* **2008,** *77*, 165107.

(28) Bilc, D. I.; Floare, C. G.; Zârbo, L. P.; Garabagiu, S.; Lemal, S.; Ghosez, P., First-principles modeling of $SrTiO_3$ based oxides for thermoelectric applications. *J. Phys. Chem. C* **2016,** *120*, 25678-25688.

(29) García-Fernández, P.; Ghosh, S.; English, N. J.; Aramburu, J. A., Benchmark study for the application of density functional theory to the prediction of octahedral tilting in perovskites. *Phys. Rev. B: Condens. Matter Mater. Phys.* **2012,** *86*, 144107.

(30) CRYSTAL Basis Sets Library. http://www.crystal.unito.it/basis-sets.php (accessed May 2019).

(31) Luo, W.-Q.; Shen, Z.-Y.; Li, Y.-M.; Wang, Z.-M.; Liao, R.-H.; Gu, X.-Y., Structural characterizations, dielectric properties and impedance spectroscopy analysis of $Nd_xSr_{1-1.5x}TiO_3$ ceramics. *J. Electroceram.* **2013,** *31*, 117-123.

(32) van Benthem, K.; Elsässer, C.; French, R. H., Bulk electronic structure of $SrTiO_3$: Experiment and theory. *J. Appl. Phys.* **2001,** *90*, 6156-6164.

(33) Shirai, K.; Yamanaka, K., Mechanism behind the high thermoelectric power factor of $SrTiO_3$ by calculating the transport coefficients. *J. Appl. Phys.* **2013,** *113*, 053705.

(34) Woodward, P. M., Octahedral tilting in perovskites. I. Geometrical considerations. *Acta Cryst.* **1997,** *B53*, 32-43.

(35) Woodward, P. M., POTATO - A program for generating perovskite structures distorted by tilting of rigid octahedra. *J. Appl. Cryst.* **1997,** *30*, 206-207.

(36) Madsen, G. K. H.; Carrete, J.; Verstraete, M. J., BoltzTraP2, a program for interpolating band structures and calculating semi-classical transport coefficients. *Comput. Phys. Commun.* **2018,** *231*, 140-145.

(37) Wang, D.; Shi, W.; Chen, J.; Xi, J.; Shuai, Z., Modeling thermoelectric transport in organic materials. *Phys. Chem. Chem. Phys.* **2012,** *14*, 16505-16520.

(38) Corà, F.; Catlow, C. R. A., QM investigations on perovskite-structured transition metal oxides: bulk, surfaces and interfaces. *Faraday Discuss.* **1999,** *114*, 421-442.

(39) Sun, J.; Singh, D. J., Thermoelectric properties of n-type $SrTiO_3$. *APL Mater.* **2016,** *4*, 104803.

(40) Mahan, G. D.; Sofo, J. O., The best thermoelectric. *Proc. Natl. Acad. Sci. U. S. A.* **1996,** *93*, 7436-7439.

For Table of Contents (TOC) Only

Twofold Increase of Power Factor with Octahedral Tilting